Wiener filtering of aliased imagery

Samuel T. Thurman* and James R. Fienup
The Institute of Optics, University of Rochester, Rochester NY 14627

ABSTRACT

We analyze a Fourier-domain Wiener filter for the reconstruction of aliased imagery. The filter is designed to minimize the expected mean square error for the unaliased portion of the object Fourier transform. This analysis yields a net system transfer function, which characterizes the combined effects of the imaging system, sampling, and the reconstruction process, that is valid at both aliased and unaliased spatial frequencies. This transfer function provides insight into how aliasing artifacts are modified by the reconstruction process. Additionally, the net transfer function is useful for characterizing the combined performance of the imaging system and post processing. For example, the net system transfer function can be used to calculate the edge response for reconstructed imagery even in the presence of aliasing. Examples are used to illustrate these aspects of using the Wiener filter with aliased imagery.

Keywords: image reconstruction, optical transfer function, aliasing

1. INTRODUCTION

Imaging systems are commonly undersampled due to signal-to-noise ratio (SNR) [1] and field of view considerations. However, many of the image reconstruction algorithms presented in the open literature are formulated for unaliased imagery. This raises a number of questions. How applicable are such algorithms to aliased imagery? How do these algorithms enhance or suppress aliasing artifacts? Does the concept of a net transfer function describing the combined effects of the imaging system and reconstruction remain valid when aliasing is present? This paper answers these questions.

Section 2 provides a mathematical foundation for analyzing the reconstruction of aliased imagery. Section 3 analyzes the effect of a linear reconstruction algorithm, in which a reconstruction is obtained by convolving an aliased image with a reconstruction kernel, on the unaliased portion of the image, aliasing artifacts, and noise. This analysis yields a net transfer function that characterizes the combined effect of the imaging system and the reconstruction process. Section 4 discusses a Wiener reconstruction algorithm that properly accounts for aliasing artifacts. Section 5 presents a number of examples that illustrate the benefits of our analysis. Section 6 is a summary. Reference [2] discusses various aspects of this work in greater detail.

2. ALIASED IMAGERY

For convenience, the analysis is presented in 1D. The extension to 2D is straightforward. Let $f(x)$ represent the intensity of an incoherent object being imaged by an isoplanatic system with incoherent point spread function $s(x)$ and detector pixel pitch p. The recorded digital image g_m is given by

$$g_m = n_m + \int_{-\infty}^{\infty} f(x,y)\, s(mp - x)\, \mathrm{d}x \quad \text{for all } m \in \{-M/2, ..., (M-2)/2\}, \tag{1}$$

where m is a sample index, M is the number of image samples, and n_m is a zero-mean, random process that represents measurement noise. Note that the effect of finite-area detector pixels can be included in $s(x)$. The discrete Fourier transform (DFT) G_u of the recorded image, given by

*thurman@optics.rochester.edu; phone 1 585 275-8008

Image Reconstruction from Incomplete Data V, edited by Philip J. Bones, Michael A. Fiddy, Rick P. Millane,
Proc. of SPIE Vol. 7076, 70760J, (2008) · 0277-786X/08/$18 · doi: 10.1117/12.794994

$$G_u = \frac{1}{\sqrt{M}} \sum_{m=-M/2}^{(M-1)/2} g_m \exp\left(-i2\pi \frac{mu}{M}\right) \quad \text{for all } u \in \{-M/2, ..., (M-2)/2\}, \tag{2}$$

can be written as [2]

$$G_u = G_{\mathrm{o},u} + G_{\mathrm{a},u} + N_u, \tag{3}$$

where $G_{\mathrm{o},u}$ is the unaliased portion of the image, given by

$$G_{\mathrm{o},u} \approx \frac{1}{p\sqrt{M}} S\left(\frac{u}{pM}\right) F\left(\frac{u}{pM}\right), \tag{4}$$

$G_{\mathrm{a},u}$ is the aliased portion of the image, given by

$$G_{\mathrm{a},u} \approx \frac{1}{p\sqrt{M}} \sum_{\substack{k=-\infty \\ k\neq 0}}^{\infty} S\left(\frac{u-kM}{pM}\right) F\left(\frac{u-kM}{pM}\right), \tag{5}$$

N_u is the DFT of n_m, $S(f_x)$ is the transfer function for the imaging system [given by the continuous Fourier transform of $s(x)$], and $F(f_x)$ is the continuous Fourier transform of the object $f(x)$. The approximations involved in Eqs. (4) and (5) arise from ignoring the effect of only have data for a finite number M of pixels. Each k term in Eq. (5) represents an alias copy of the continuous Fourier transform of the image being recorded.

3. RECONSTRUCTION OF ALIASED IMAGERY

We consider the case of a general linear reconstruction algorithm, in which a reconstruction $\hat{f}_m$ is formed as a discrete circulant convolution of the aliased image g_m with a reconstruction filter w_m, *i.e.*,

$$\hat{f}_m = \frac{1}{\sqrt{M}} \sum g_{m'} w_{m-m'}. \tag{6}$$

In the Fourier domain, the reconstruction can be expressed as

$$\hat{F}_u = W_u G_u, \tag{7}$$

where $\hat{F}_u$, G_u, and W_u are the corresponding DFTs of $\hat{f}_m$, g_m, and w_m, respectively. Substituting Eqs. (3), (4), and (5) into Eq. (7) yields

$$\hat{F}_u = W_u N_u + \frac{W_u}{p\sqrt{M}} \sum_{k=-\infty}^{\infty} S\left(\frac{u-kM}{pM}\right) F\left(\frac{u-kM}{pM}\right). \tag{8}$$

Let $\Omega(f_x)$ represent a continuous periodic extension of W_u, defined such that

$$W_u = \Omega\left(\frac{u}{pM}\right) \tag{9}$$

and

$$\Omega(f_x) = \Omega\left(f_x - \frac{k}{p}\right) \quad \text{for } k \in \{0, \pm 1, \pm 2, ...\}. \tag{10}$$

Now, Eq. (8) can be written as

$$\hat{F}_u = W_u N_u + \frac{1}{p\sqrt{M}} \sum_{k=-\infty}^{\infty} S_{\mathrm{net}}\left(\frac{u-kM}{pM}\right) F\left(\frac{u-kM}{pM}\right), \tag{11}$$

where

$$S_{\text{net}}\left(f_x\right) = \Omega\left(f_x\right) S\left(f_x\right), \tag{12}$$

is a net transfer function that describes the combined effect of imaging with $S(f_x)$, sampling, and reconstruction with W_u on the underlying signal. In other words, the unaliased and aliased signal components of the reconstruction are equivalent to the viewing the object through a system with a transfer function $S_{\text{net}}(f_x)$ and sampling. It is important to note that the expression for $S_{\text{net}}(f_x)$ is valid for aliased spatial frequencies, *i.e.*, for $f_x \le -1/(2p)$ or $f_x > 1/(2p)$. When there is no aliasing, Eq. (12) yields the well-known result that the net transfer function simply the product of the individual transfer functions of the imaging system and the reconstruction filter.

The derived net transfer function $S_{\text{net}}(f_x)$ has a number of practical uses, one of which is to calculate the normalized edge response ER(x) for the reconstructed imagery [3]. ER(x) can be used to characterize the performance of an imaging system. The edge response can be computed from $S_{\text{net}}(f_x)$ using the following expression

$$\text{ER}\left(x\right) = \frac{1}{2}\int_{-\infty}^{\infty} S_{\text{net}}\left(f_x\right)\left[\delta\left(f_x\right) - \frac{i}{\pi f_x}\right]\exp\left(\text{i}2\pi x f_x\right)\text{d}f_x, \tag{13}$$

where $\delta(f_x)$ is the Dirac delta function. A standard approach for characterizing an imaging system is to: (i) extract ER(x) from the image of an edge and (ii) use the extracted ER(x) to estimate $S_{\text{net}}(f_x)$. For aliased imagery, the edge needs to be tilted with respect to the image coordinates. ER(x) is also used to compute the relative edge response RER of an imaging system as

$$\text{RER} = \text{ER}\left(p/2\right) - \text{ER}\left(-p/2\right). \tag{14}$$

RER is a measure of the spatial resolution of an imaging system with respect to pixel pitch. RER plays a significant role in determining overall image quality.

4. WIENER FILTER FOR ALIASED IMAGERY

The Wiener filter [4-8] is a particularly attractive reconstruction algorithm for a number of reasons. It is simple to implement and computationally efficient, yet it yields results that are better than or comparable to more complex, iterative algorithms [8]. In Reference [2], we derived a Fourier-domain Wiener filter that properly accounts for aliasing. Prior implementations exist for the aliased imagery [7], but these are formulated in the spatial domain as the solution to a large matrix equation and do not offer much physical insight. Working in the Fourier domain has the advantage of being able to easily distinguish terms associated with the unaliased portion of the underlying signal, aliasing artifacts, and noise. Specifically, the Fourier-domain Wiener filter $W(u,v)$ can be written as [2]

$$W_u = \frac{S^*\left[u/(pM)\right]\Phi_{\text{o}}\left[u/(pM)\right]}{\left|S\left[u/(pM)\right]\right|^2\Phi_{\text{o}}\left[u/(pM)\right] + c_{\text{a}}\Phi_{\text{a}}\left[u/(pM)\right] + c_{\text{n}}\Phi_{\text{n}}\left[u/(pM)\right]}, \tag{15}$$

where $\Phi_{\text{o}}(f_x)$, $\Phi_{\text{a}}(f_x)$, and $\Phi_{\text{n}}(f_x)$ are power spectra for the object being imaged, aliasing artifacts in the measured image, and noise in the measured image, respectively. The parameters c_{a} and c_{n} in Eq. (13) are used to control the trade-offs between edge sharpness, artifact suppression, and noise gain in the reconstructed image. With $c_{\text{a}} = c_{\text{n}} = 1$, the Wiener filter of Eq. (13) yields a reconstruction with the minimum expected mean-squared error for the unaliased portion of the object Fourier transform, *i.e.*, the following error measure is minimized

$$\left\langle e\right\rangle = \left\langle \sum_{u=-M/2}^{(M-2)/2}\left|\hat{F}_u - F\left(\frac{u}{pM}\right)\right|^2\right\rangle, \tag{16}$$

where the angle brackets represent and expectation value computed with respect to both the noise and object statistics (the image is considered to be a stochastic process).

A practical model [9-13] for the unaliased object power spectrum is

$$\Phi_{\mathrm{o}}(\rho)=\begin{cases}A_0^2 & \text{for } \rho=0\\ A^2\rho^{-2\alpha} & \text{for } \rho>0\end{cases}, \tag{17}$$

where ρ is a radial spatial-frequency coordinate in two dimensions, and A_0, A and α are parameters of the model. Keeping with 1D notation, the power spectrum for the aliased artifacts in the unprocessed image g_m can be written as

$$\Phi_{\mathrm{a}}(f_x)=\sum_{\substack{k=-\infty\\ k\neq 0}}^{\infty}\left|S\left(f_x-\frac{k}{p}\right)\right|^2\Phi_{\mathrm{o}}\left(f_x-\frac{k}{p}\right), \tag{18}$$

when the object is wide-sense stationary, as is often assumed for Fourier-domain Wiener filter implementations [6,7]. The noise is nearly white for typical imaging scenarios, such that $\Phi_{\mathrm{n}}(f_x) = \Phi_{\mathrm{n}}$, a constant, is a good approximation. Reference [2] outlines a method for estimating the various power spectrum parameters A_0, A, α and Φ_{n} for noisy, aliased imagery that accounts for both $S(f_x)$ and aliasing. This method was used to obtain the results in Section 5.

5. EXAMPLES

This section examines a number of examples using simulated data to illustrate various aspects of Wiener filtering aliased imagery. Figure 1 shows the object $f(x)$ used for the simulations. Figure 2(a) shows a simulated image g_m for an unaberrated imaging system with a circular pupil, operating at λ FN/p = 1, where FN is the system f-number. Figures 2(b), 2(c) and 2(d) show the image contributions due to the unaliased portion of the image, aliasing artifacts, and noise, respectively. These are the spatial-domain counter parts of $G_{\mathrm{o},u}$, $G_{\mathrm{a},u}$, and N_u, respectively. The simulation included shot noise only, and the average number of photons per pixel in the image was 30,000. Figures 2(a) and 2(b) are displayed using the same grayscale as Fig. 1, while Figs. 2(c) and 2(d) use a grayscale stretched by a factor of 5. The effect of aliasing is particularly noticeable in the upper left corner of the image, where the finely-spaced diagonal lines on the parking lot pavement appear to be orieneted in the wrong direction when compared to the actual object shown in Fig. 1.

Fig. 1. Object $f(x)$ used for simulation examples [14].

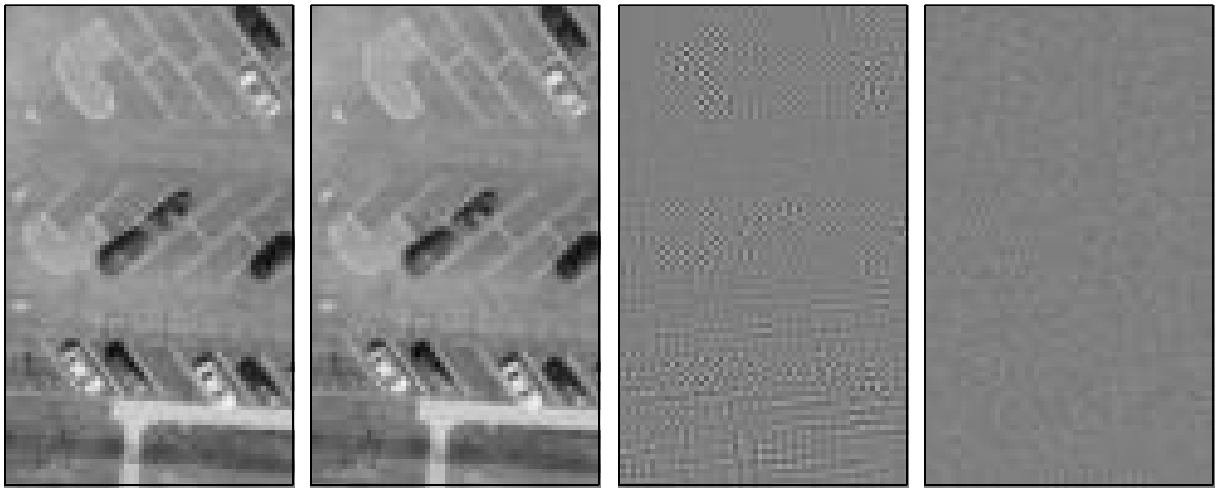

(a) (b) (c) (d)

Fig. 2. (a) Simulated image g_{m} for the unaberrated imaging system and its various contributions due to the (b) unaliased portion of the image, (c) aliasing artifacts, and (d) noise. Figures 2(b)-2(d) are the spatial-domain counterparts of $G_{\mathrm{o},u}$, $G_{\mathrm{a},u}$, and N_u, respectively.

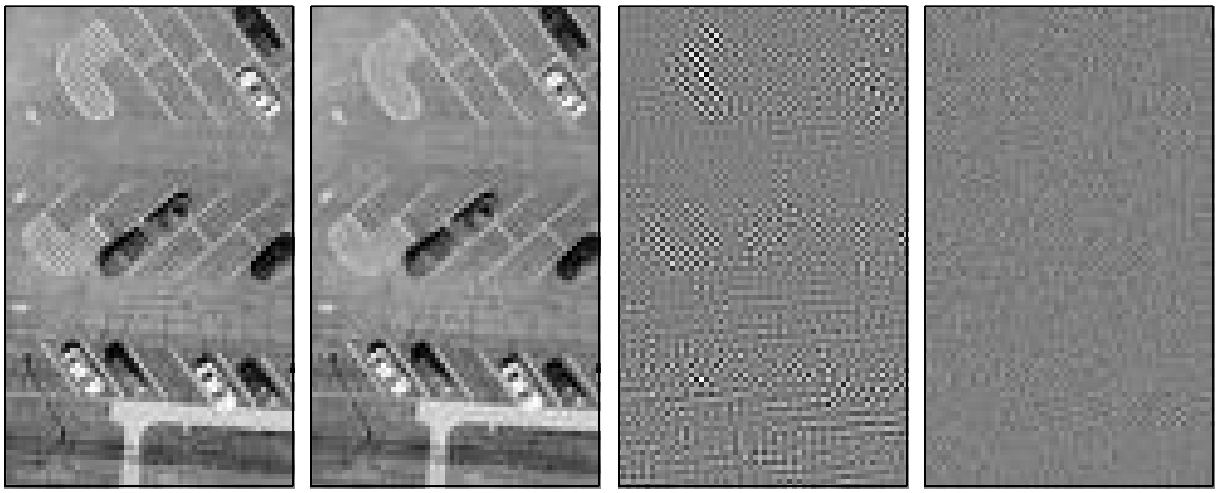

(a) (b) (c) (d)

Fig. 3. (a) Wiener reconstruction $\hat{f}_m$ of Fig. 2(a) using $c_{\mathrm{n}} = c_{\mathrm{a}} = 0.2$, and the various components of the reconstruction associated with the (b) unaliased portion of the image, (c) aliasing artifacts, and (d) noise. Figures 3(a)-3(d) were obtained by convolving Figures 2(a)-2(d) with the Wiener filter kernel w_m.

Figure 3 shows the Wiener reconstruction $\hat{f}_m$ of the data in Fig. 2 using $c_{\mathrm{n}} = c_{\mathrm{a}} = 0.2$. In addition to increasing the sharpness of edges in the reconstruction, the Wiener filter also amplifies the aliasing artifacts and noise. Figure 4 demonstrates the fact that the unalaised and aliased portions of the reconstruction can be computed equivalently using the net transfer function $S_{\mathrm{net}}(f_x)$. Figure 5 demonstrates how aliasing artifacts can be suppressed in the reconstruction at the expense of reduced edge sharpness by using a larger value of $c_{\mathrm{a}} = 10$.

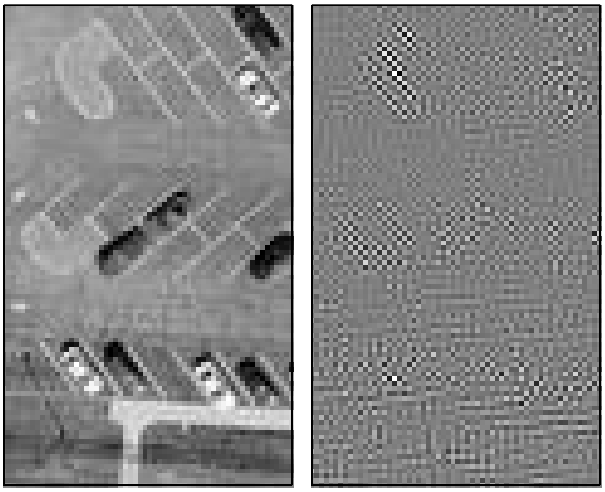

(a) (b)

Fig. 4. Contributions to the Wiener reconstruction shown in Fig. 2(a) associated with the (a) unaliased portion of the image and (b) aliasing artifacts. Figures 4(a) and 4(b) are identical to Figures 3(b) and 3(c), but were computed by passing the object $f(x)$ through the net transfer function $S_{\text{net}}(f_x)$ and then sampling.

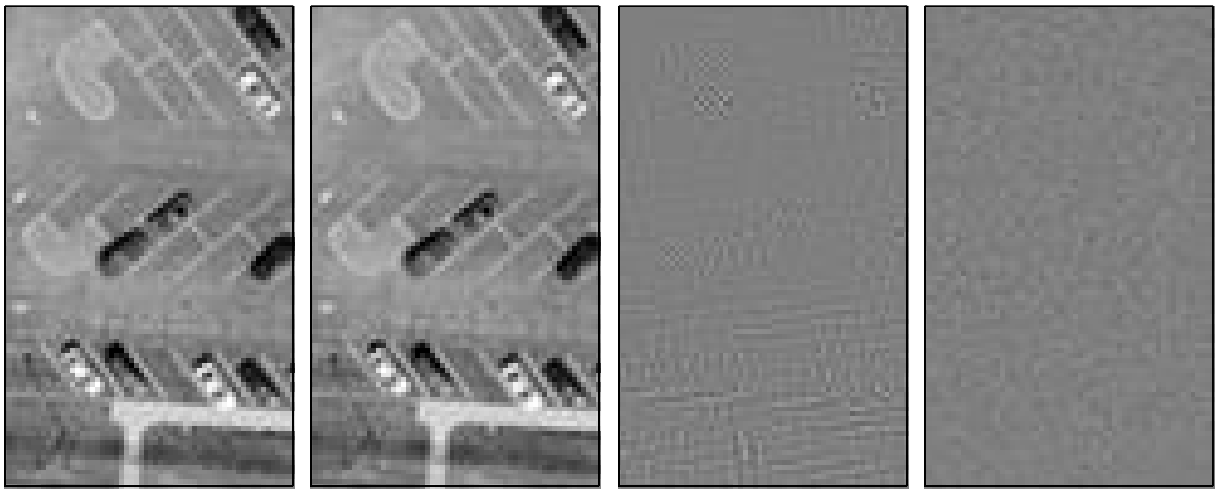

(a) (b) (c) (d)

Fig. 5. (a) Wiener reconstruction $\hat{f}_m$ of Fig. 2(a) using $c_{\text{n}} = 0.2$ and $c_{\text{a}} = 10$, and the various components of the reconstruction associated with the (a) unaliased portion of the image, (b) aliasing artifacts, and (c) noise.

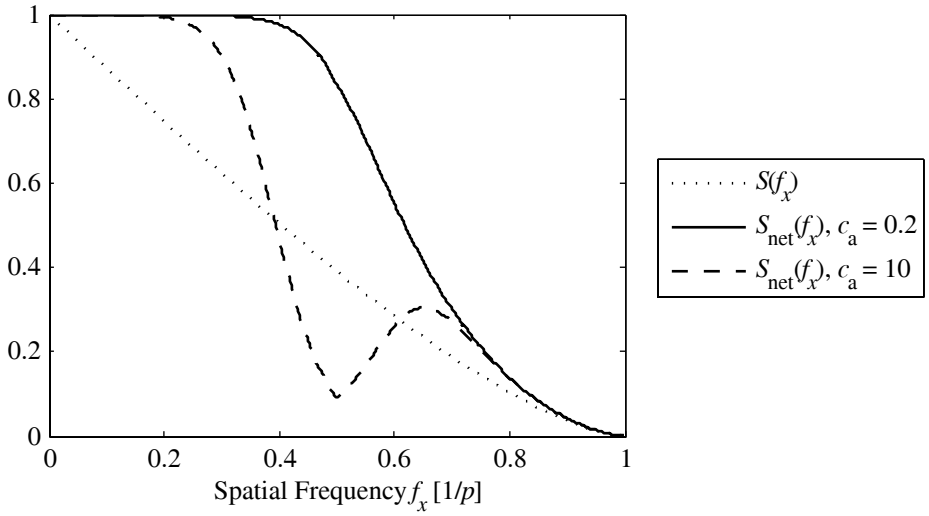

Fig. 6. The transfer function $S(f_x)$ for the unaberrated imaging system (dotted line) and the net transfer functions $S_{net}(f_x)$ that include the effect of the Wiener filter used in reconstructing Fig. 3(a) (solid line) and Fig. 5(a) (dashed line).

Figure 6 shows cuts through the transfer function $S(f_x)$ of the unaberrated imaging system and the net transfer functions $S_{net}(f_x)$ for both values of $c_a = 0.2$ and 10. For the smaller value of $c_a = 0.2$, the Wiener filter W_u boosts $S_{net}(f_x)$ up to near unity for spatial frequencies $|f_x| \leq 1/(2p)$. The form of $S_{net}(f_x)$ for higher spatial frequencies $|f_x| > 1/(2p)$ that are aliased results from the product of $S(f_x)$ with the particular values of W_u used to compensate for the transfer function of the imaging system $S(f_x)$ at lower, unaliased spatial frequencies. Mathematically, the coupling between $S_{net}(f_x)$ at aliasied and unaliased spatial frequencies due to W_u is described by the function $\Omega(f_x)$, which is a periodic extension of W_u along f_x. For the larger value of $c_a = 10$, the Wiener filter boosts $S_{net}(f_x)$ less in favor of better suppression of the aliasing artifacts.

Next, we illustrate the practical uses of $S_{net}(f_x)$ mentioned in Section 4. Figure 7(a) shows a noiseless simulated image of a tilted edge for the unaberrated imaging system, while Fig. 7(b) shows a reconstruction with the same Wiener filter used to obtain the results shown in Fig. 3 with $c_n = c_a = 0.2$. Figure 8 shows the normalized edge response ER(x) of the unaberrated imaging system obtained by two methods: (i) extraction from the image of Fig. 7(a) and (ii) direct computation from $S(f_x)$ using Eq. (13). Note that both methods yield identical forms of ER(x). Figure 9 shows the normalized edge response ER(x) for the reconstructed image of Fig. 7(b), again obtained by extraction from the aliased imagery and by direct computation using $S_{net}(f_x)$. As expected, the edge responses agree. Additionally, the relative edge response RER of a system can be computed using Eq. (14). Without reconstruction, a value of RER = 0.692 was computed using $S(f_x)$. Including the effect of the Wiener filter, values of RER = 0.995 and 0.776 were computed for c_a = 0.2 and 10, respectively, using $S_{net}(f_x)$.

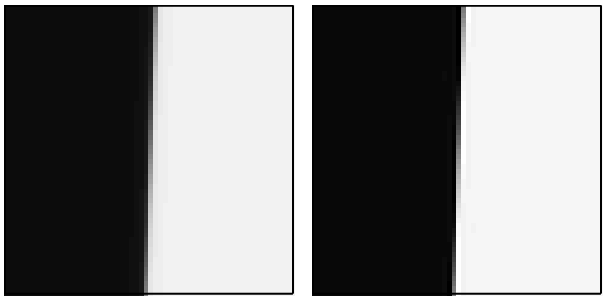

Fig. 7. (a) Simulated image g_m of an edge tilted by 2° with respect to the image coordinates and (b) the reconstruction $\hat{f}_m$ of Fig.6(a) obtained by applying the same Wiener filter used to reconstruct Fig. 3(a).

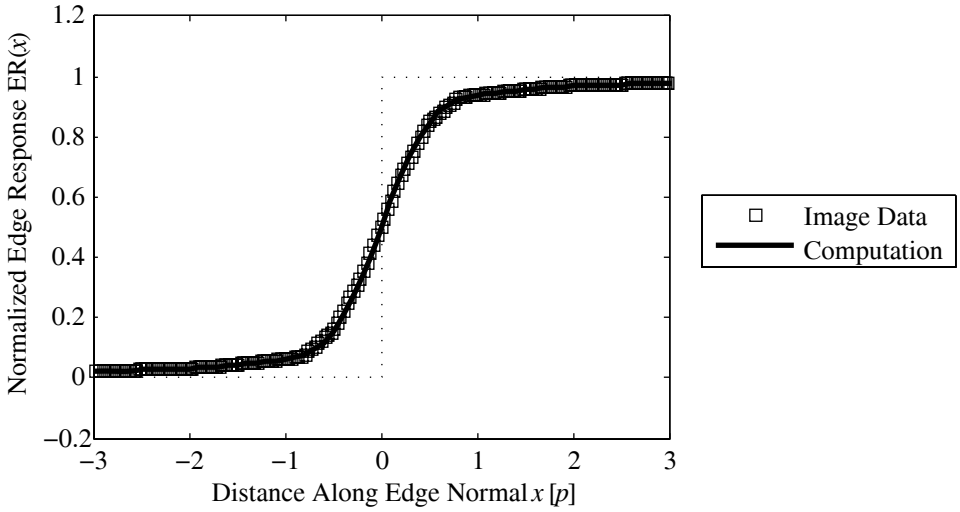

Fig. 8. Normalized edge response ER(x) for the unaberrated imaging system obtained by extraction from the image shown in Fig. 7(a) (squares) and direct computation using $S(f_x)$ (solid line).

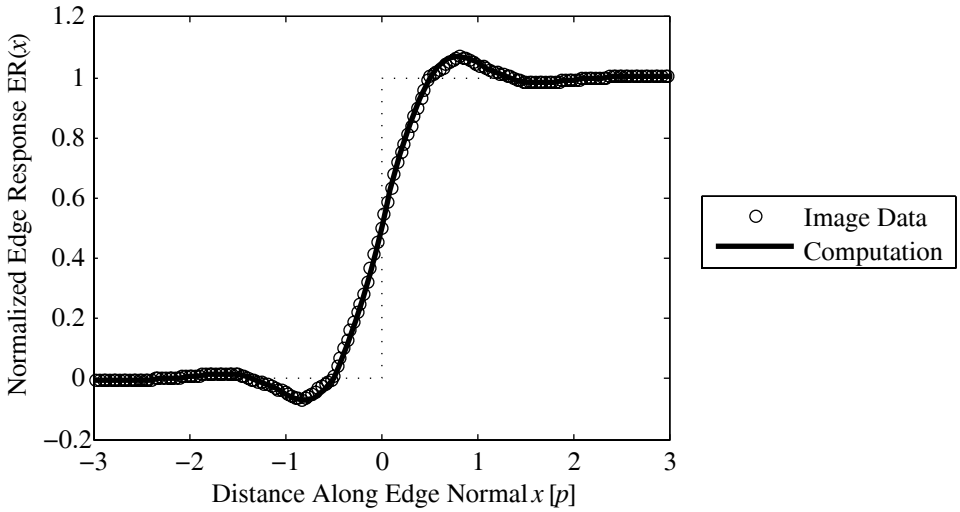

Fig. 9. Normalized edge response ER(x) for the Wiener filtered imagery from the unaberrated system obtained by extraction from the image shown in Fig. 7(b) (circles) and direct computation using $S_{\text{net}}(f_x)$ (solid line).

For the last example, we consider an aberrated imaging system. Figure 10 shows the pupil wavefront aberration function used for this purpose. This wavefront aberration function was obtained by: (i) generating a random-draw atmospheric phase screen with Komolgorov statistics [15], (ii) subtracting piston, tip, and tilt phase terms across the pupil, and (iii) scaling the amplitude of the phase screen to have a root-mean-squared phase error of $\lambda/5$ (the resulting peak-to-valley phase error was 1.04λ). Figure 11 shows a simulated image g_m with an average number of 80,000 photons per pixel. Figure 12 shows the Wiener reconstruction results for $c_{\text{n}} = c_{\text{a}} = 0.2$. Figure 13 shows the modulation transfer function $|S(f_x)|$ of the aberrated imaging system and the net modulation transfer function $|S_{\text{net}}(f_x)|$ for the reconstructed imagery. Notice that $|S_{\text{net}}(f_x)| > 1$ for a number of aliased spatial frequencies. This is due to combined effects of the aggressive boosting needed to compensate for $S(f_x)$ at unaliased spatial frequencies and the relatively small penalty associated with aliasing artifacts for $c_{\text{a}} = 0.2$. One could adjust the values of c_{a} and c_{n} could to obtain a reconstruction suited to personal liking.

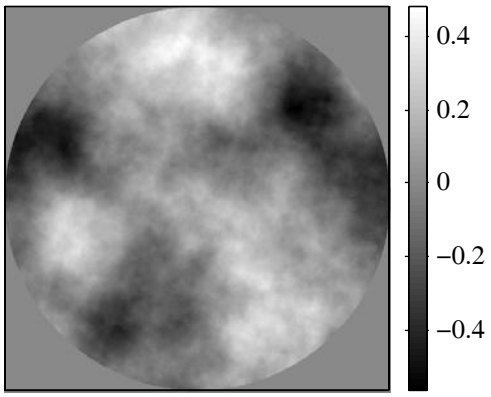

Fig. 10. Wavefront aberration function in units of waves for the aberrated imaging system.

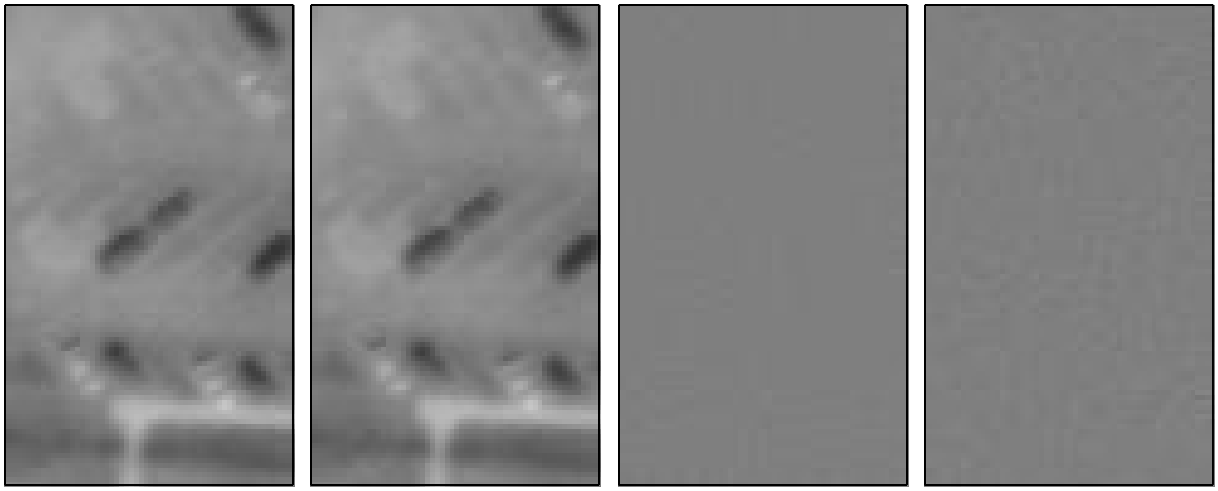

Fig. 11. (a) Simulated image g_m for the aberrated imaging system and its various contributions due to the (b) unaliased portion of the image, (c) aliasing artifacts, and (d) noise.

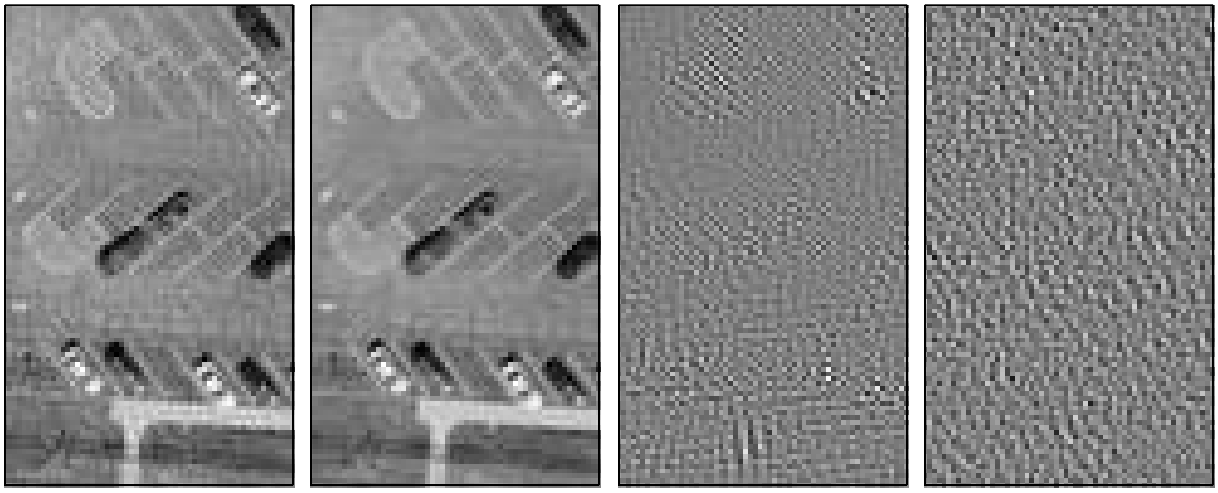

(a) (b) (c) (d)

Fig. 12. (a) Wiener reconstruction $\hat{f}_m$ of Fig. 10(a) using $c_n = c_a = 0.2$, and the various components of the reconstruction associated with the (a) unaliased portion of the image, (b) aliasing artifacts, and (c) noise.

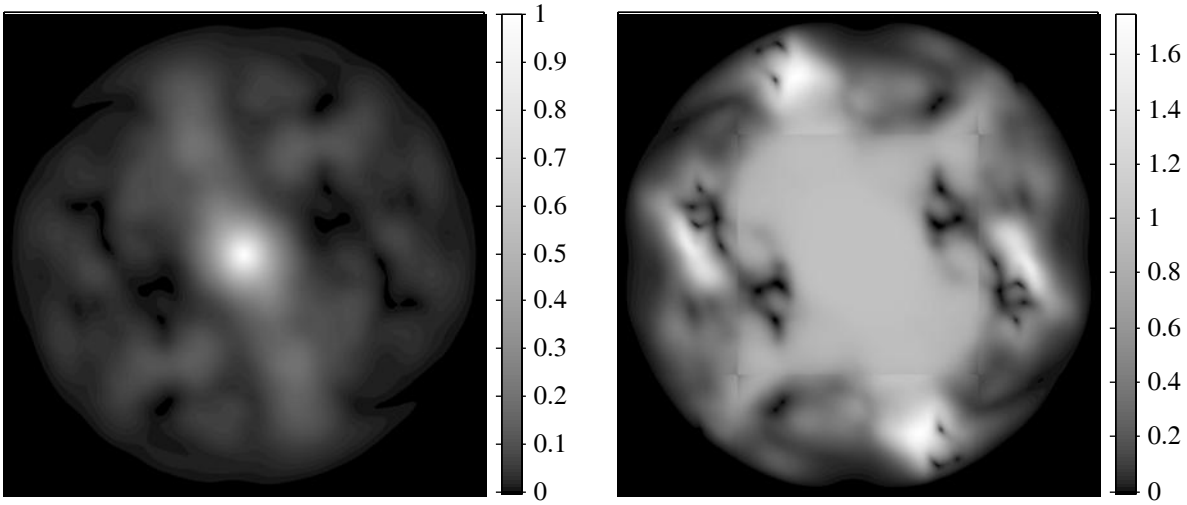

(a) (b)

Fig. 13. (a) The modulation transfer function $|S(f_x)|$ of the aberrated imaging system and (b) the net modulation transfer function $S_{net}(f_x)$, which includes the effects of the Wiener filter used in reconstructing Fig. 12(a).

6. SUMMARY

It is apparent that one can sensibly apply linear reconstruction algorithms to aliased imagery. The analysis of Section 3 provides insight into how such algorithms affect the various components of an image, namely the unaliased portion of an image, aliasing artifacts, and noise. A net transfer function that describes the combined effects of an imaging system, sampling, and the reconstruction process was derived. A Fourier-domain Wiener filter that properly accounts for aliasing artifacts was presented in Section 4. The Wiener filter contains parameters that can be used to adjust the trade-offs between edge sharpness, suppression of aliasing artifacts, and noise gain for the reconstruction. A number of examples were discussed in Section 5 to illustrate the features of the Wiener filtering algorithm and point out the practical uses of the net transfer function.

ACKNOWLEDGEMENT

This work was supported by the U.S. Department of Defense.

REFERENCES

[1] R. D. Fiete, "Image quality and λFN / p for remote sensing systems," Opt. Eng. **38**, 1229-1240 (1999).
[2] S. T. Thurman and J. R. Fienup, "Wiener reconstruction of undersampled imagery," (to be submitted to J. Opt. Soc. Am. A).
[3] J. C. Leachtenauer, W. Malila, J. Irvine, L. Colburn, and N. Salvaggio, "General Image-Quality Equation: GIQE," Appl. Opt. **36**, 8322-8328 (1997).
[4] N. Wiener, *Extrapolation, Interpolation and Smoothing of Stationary Time Series*, (John Wiley & Sons, New York, 1950).
[5] H. W. Bode and C. E. Shannon, "A simplified derivation of linear least square smoothing and prediction theory," Proc. IRE **38**, 417-425 (1950).
[6] C. W. Helstrom, "Image reconstruction by the method of least squares," J. Opt. Soc. Am. **57**, 297-303 (1967).
[7] A. K. Jain, *Fundamentals of Digital Image Processing*, (Prentice Hall, Englewood Cliffs, NJ, 1989).
[8] J. R. Fienup, D. Griffith, L. Harrington, A. M. Kowalczyk, J. J. Miller, and J. A. Mooney, "Comparison of Reconstruction Algorithms for Images from Sparse-Aperture Systems," Proc. SPIE **4792**, 1-8 (2002).
[9] N. G. Deriugin, "The power spectrum and the correlation function of the television signal," Telecommunications **1**, 1-12 (1956).
[10] G. J. Burton and I. R. Moorhead, "Color and spatial structure in natural scenes," Appl. Opt. **26**, 157-170 (1987).
[11] D. J. Tolhurst, Y. Tadmor, and T. Chao, "Amplitude spectra of natural images," Opthal. Physiol. Opt. **12**, 229-232 (1992).
[12] D. L. Ruderman and W. Bialek, "Statistics of natural images: Scaling in the woods," Phys. Rev. Lett. **73**, 814-817 (1994).
[13] A. van der Schaaf and J. H. van Hateren, "Modeling the power spectra of natural images: statistics and information," Vision Res. **36**, 2759-2770 (1996).
[14] This image is public domain and is available through the URL http://seamless.usgs.gov/.
[15] R. G. Lane, A. Glindemann and J. C. Dainty, "Simulation of a Kolmorgorov phase screen," Waves in Random Media **2**, 209-224 (1992).